

## Article

# Al<sub>2</sub>O<sub>3</sub> Coatings for Protection of Stainless Steel 316L against Corrosion in Zn-Al and Zn-Al-Mg

Giovanni Paolo Alparone <sup>1,\*</sup>, David Penney <sup>1</sup> , James Sullivan <sup>1</sup>, James Edy <sup>2</sup> and Christopher Mills <sup>2</sup> <sup>1</sup> Department of Materials Engineering, Swansea University, Swansea SA2 8PP, UK<sup>2</sup> Tata Steel, Research and Development, Swansea Technology Centre, Swansea SA2 8PP, UK

\* Correspondence: 2043556@swansea.ac.uk

**Abstract:** The production and quality of automotive-grade galvanised steel are affected by the limited service life of the pot roll bearings used in continuous galvanising lines. The journal bearings are subjected to severe degradation as they react with the molten Zn bath, and coatings can provide corrosion protection to the bearing materials. This research investigates the performance of Al<sub>2</sub>O<sub>3</sub> coatings applied via the HVOF thermal spray process to stainless steel 316L substrates. Immersion tests were conducted in baths of different compositions, namely GI (Zn-0.3 wt.% Al) and ZMA (Zn-1.5 wt.% Al-1.5 wt.% Mg). Material characterisation after testing showed evidence of coating degradation after 1 week, as the coating tended to crack and detach from the substrate, allowing the molten Zn to attack the underlying steel. The coefficient of thermal expansion of Al<sub>2</sub>O<sub>3</sub> and steel was measured, and a difference of  $13 \times 10^{-6} \text{ K}^{-1}$  was found, leading to the development of cracks in the coatings. Zn penetration through cracks was determined to be the main failure mechanism of the Al<sub>2</sub>O<sub>3</sub> coatings, which otherwise remained inert to Zn-Al. Conversely, the coatings immersed in Zn-Al-Mg reacted with the Mg in the molten metal bath, showing that changing bath composition affected the performance of the coatings in molten Zn alloy.

**Keywords:** ceramics; corrosion; thermal expansion; continuous galvanising; pot hardware; pot roll journal bearings



**Citation:** Alparone, G.P.; Penney, D.; Sullivan, J.; Edy, J.; Mills, C. Al<sub>2</sub>O<sub>3</sub> Coatings for Protection of Stainless Steel 316L against Corrosion in Zn-Al and Zn-Al-Mg. *Coatings* **2024**, *14*, 606. <https://doi.org/10.3390/coatings14050606>

Academic Editor: Chi Tat Kwok

Received: 16 April 2024

Revised: 30 April 2024

Accepted: 9 May 2024

Published: 11 May 2024



**Copyright:** © 2024 by the authors. Licensee MDPI, Basel, Switzerland. This article is an open access article distributed under the terms and conditions of the Creative Commons Attribution (CC BY) license (<https://creativecommons.org/licenses/by/4.0/>).

## 1. Introduction

Depending on customer requirements, different Zn-based coatings can be produced on a continuous galvanising line. For example, automotive steel customers demand high surface quality standards, especially for visible parts, which must be free of imperfections before and after forming processes [1]. This is particularly important as the subsequently painted panels play an important role in the decision-making process for purchasing a car [2]. Galvanised steel products which are therefore intended for use within the automotive sector require stringent quality control to ensure that the surface has minimal defects and achieves the desired surface roughness tolerance. As a result, automotive customers require a galvanised steel product with a high quality surface finish, which is typically referred to as ‘full-finish’ galvanised steel and is characterised by the Zn-Al composition of the galvanised coating.

In the galvanising process, the pot hardware, which includes the pot rolls and the roll journal bearings, guides the strip steel through the bath of liquid Zn alloy. The stability of the strip through the bath is considered to be key to the quality of automotive-grade galvanised products and is related to pot furniture performance. The roll bearings are submerged in the hot dip galvanised bath and are exposed to chemical attack by the liquid Zn alloy at temperatures over 400 °C [3–6]. The deterioration of the surface of the bearings, under the action of the liquid Zn alloy, is responsible for causing vibrations in the strip steel as it emerges from the bath and passes through gas knives, where the thickness of the Zn coating is controlled. These vibrations lead to defects in the coating, affecting the quality of

the final product [6]. As a result, the service time of the roll bearings is typically limited to five weeks before the pot rolls and bearings are changed and reconditioned. These changes lead to down time on the line and a restriction on the production window for premium ‘full-finish’ products. Therefore, the consequence of degraded pot roll journal bearings is down time, quality issues and loss of yield [7,8]. Achieving a reduction in the maintenance ‘down days’ by extending the lifetime of the pot hardware is, therefore, of financial benefit to the galvanising industry.

Stainless steel 316L (SS 316L) is a material of choice for the fabrication of galvanising pot hardware as it provides good corrosion resistance in molten Zn at a convenient price. However, SS 316L is not inert in liquid Zn alloys. Fe-Al phases can form on the surface of the steel for baths with Al content above 0.15 wt.%, for example [9]. Investigations have confirmed that the SS 316L sleeves of a sink roll system can corrode in liquid Zn, leading to the formation of intermetallic phases that influence the wear of the bearing surface [10]. The accumulation of intermetallic phases onto the bearing surface can reduce the clearance between the journal sleeve and bushing components of the bearings, resulting in a ‘lock-up’ of these components. Moreover, the breakdown and spallation of the reaction layers are detrimental to the lifetime of the bearings components, as abrasive particles develop and subsequently damage the bearings [4]. It is clear that chemical inertness to molten Zn is a requirement for developing journal bearings with extended service life. The aim of this study is to develop a coating inert to liquid Zn alloy that can protect SS 316L from the attack of molten metal. The application of such coating will enable a significant reduction in down time on the line and extend the production window of a ‘full-finish’ product with high financial reward.

Various coatings have been examined as a method for developing bearings with extended durability, and thermal sprayed coatings consisting of WC particles embedded in a Co- or Fe-based matrix have previously been applied to the bearings to enhance their wear resistance. However, the matrix supporting the WC particles was observed to react with liquid Zn alloy, leading to cracking of the WC particles and failure of the coating [4,10]. Ceramic materials show promise due to their inertness in molten metal [11–15]. For example, recent research showed that aluminium oxide ( $\text{Al}_2\text{O}_3$ ) is inert to liquid Zn-Al [11]. As such,  $\text{Al}_2\text{O}_3$  coatings can potentially shield the bearing materials from the attack of liquid Zn-Al, limiting wear and the subsequent degradation of these components. In recent decades there has been an increasing interest in weight reduction within the automotive sector, primarily in order to minimise fuel consumption [16]. For this reason, the galvanising industry has introduced Zn-Al-Mg (ZAM) coatings, and, at present, the literature lacks studies on the corrosion behaviour of bearing materials in Zn-Al-Mg baths.

The present work analyses the performance of  $\text{Al}_2\text{O}_3$  coatings applied to SS 316L via High-Velocity Oxygen Fuel (HVOF) technology. The corrosion behaviour in molten Zn alloy was investigated in comparison with uncoated SS 316L to determine whether it can offer protection to stainless steel from the attack of liquid Zn-Al and Zn-Al-Mg. To achieve this, the coating must remain unreactive in molten metal and act as a barrier against diffusion of molten Zn alloy into steel. In addition to this, the  $\text{Al}_2\text{O}_3$  coatings were examined for structural integrity after exposure to molten metal at high temperatures. These investigations enabled to assess the potential of  $\text{Al}_2\text{O}_3$  coatings for application in continuous galvanising lines.

## 2. Materials and Methods

### 2.1. Materials

The specimens used in this study consisted of 20 mm × 20 mm × 5 mm plates of SS 316L, which were coated with a 250 μm thick  $\text{Al}_2\text{O}_3$  layer. The coating was applied via the HVOF thermal spray process, which was carried out by Engineered Performance Coatings (Cardiff, UK). In addition to this, as-received SS 316L plates were tested and used as benchmarks.

## 2.2. Static Immersion Testing

The corrosion performance of SS 316L with and without  $\text{Al}_2\text{O}_3$  coating was studied through static immersion in liquid Zn, meaning that the samples remained stationary during the tests. These experiments were carried out in two graphite crucibles (Figure 1) filled with 20 kg of Zn ingots, obtaining bath compositions of Zn-0.3 wt% Al (GI) and Zn-1.5 wt% Al-1.5 wt% Mg (ZAM). The specimens were suspended using SS 316L wire and preheated at 300 °C for 1 h before being submerged in each bath in order to minimise the effects of thermal shock. All the samples were submerged completely below the Zn level. The furnace temperature was maintained at 465 °C throughout the test and was monitored by thermocouples. A total of five specimens were immersed in each bath, which were removed one at a time after 1-week intervals. The last specimen was removed after 5 weeks of testing. As the samples were taken out from the molten Zn, they were allowed to cool naturally and, subsequently, pickled with HCl acid (35%) to remove the residual Zn.

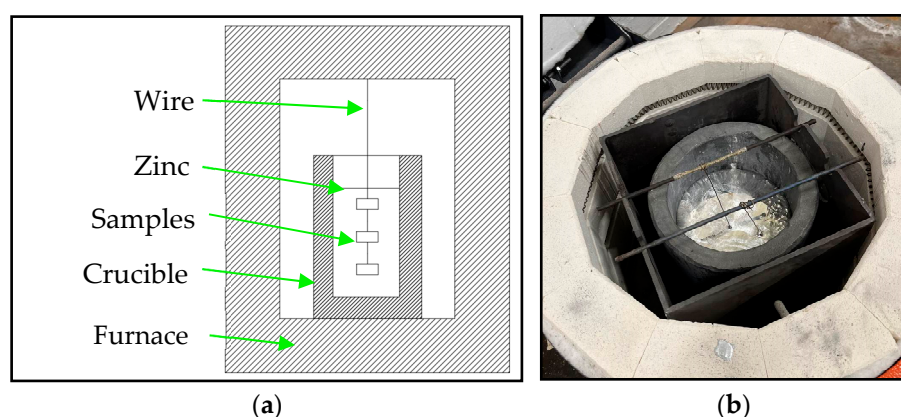


**Figure 1.** (a) Experimental setup used for static testing; (b) top loading furnace with Zn alloy bath.

## 2.3. Material Characterisation

The samples were mounted in conductive resin (CEM3070), ground with coarse SiC grit to obtain cross-sections of the specimens and polished using diamond slurries. Images of the specimens were taken before and after static testing using a ZEISS (Oberkochen, Germany) EVO scanning electron microscope (SEM) and a Hitachi (Tokyo, Japan) TM4000 desktop SEM, both equipped with backscattered electron detectors (BSD). Energy Dispersive X-ray analysis (EDS) was performed using an Oxford Instruments (Abingdon, UK) EDS Detector with Aztec 6.1 software. The  $\text{Al}_2\text{O}_3$  coatings were sputter coated with a 5 nm thick Pt layer to prevent charging. X-ray diffraction (XRD) was conducted using a Bruker (Billerica, MA, USA) D8 Discover. Diffraction patterns were collected at room temperature, over an angular range of 20° to 80° with a count time per step of 1 s and 0.03° step size. The diffraction data generated were analysed using DIFFRAC.EVA 7.0.0.4 software, and the diffraction patterns were compared to the reference patterns of known phases available in the Crystallography Open Database [17]. The coefficients of thermal expansion (CTEs) of  $\text{Al}_2\text{O}_3$  and SS 316L were determined using a NETZSCH (Selb, Germany) DIL402C dilatometer. Dilatometric curves were acquired on bars (diameter 5 mm; length 20 mm) on heating from RT to 465 °C at a rate of 10 K min<sup>-1</sup>.

## 3. Results and Discussion

### 3.1. Characterisation of Untested $\text{Al}_2\text{O}_3$ Coatings

SEM images of the as-received  $\text{Al}_2\text{O}_3$  coating obtained with the BSD detector are shown in Figure 2. The cross-section of the specimen (Figure 2a) shows a dark grey phase, which is the ceramic coating, and a light grey phase, which is the SS 316L substrate. A high-magnification image of the surface of the  $\text{Al}_2\text{O}_3$  coating is illustrated in Figure 2b, showing the presence of pores in the as-received coatings. EDS was performed on the surface of the  $\text{Al}_2\text{O}_3$  and on the SS 316L substrate to identify the elements present in the

specimen. The analysis revealed that only Al and O were present, as expected. The content of Al and O was approximately  $57 \pm 0.5$  wt.% and  $43 \pm 0.4$  wt.%, respectively, which corresponded to approximately 40 mol% for Al and 60 mol% for O; therefore, the results of EDS agreed with the expected stoichiometry. The average composition of the coating and of the SS 316L substrate is shown in Figure 3. X-ray diffraction patterns of the untested Al<sub>2</sub>O<sub>3</sub> coatings (Figure 4) allowed the identification of the phases present in the ceramic. The diffractogram showed that the majority of the peaks corresponded to hexagonal aluminium oxide (corundum); however, several peaks revealed the presence of cubic aluminium oxide (Al<sub>2.66</sub>O<sub>4</sub>). There are several variants of aluminium oxide [18], and this phase is one of the known transition phases, which is characterised by a face-centred cubic crystal (fcc) structure as opposed to the stable phase with a hexagonal close-packed (hcp) structure [19]. Other studies identified the cubic phase in Al<sub>2</sub>O<sub>3</sub> coatings and attributed its presence to the faster cooling of the Al<sub>2</sub>O<sub>3</sub> particles hitting the target substrate during the thermal spray process [11].

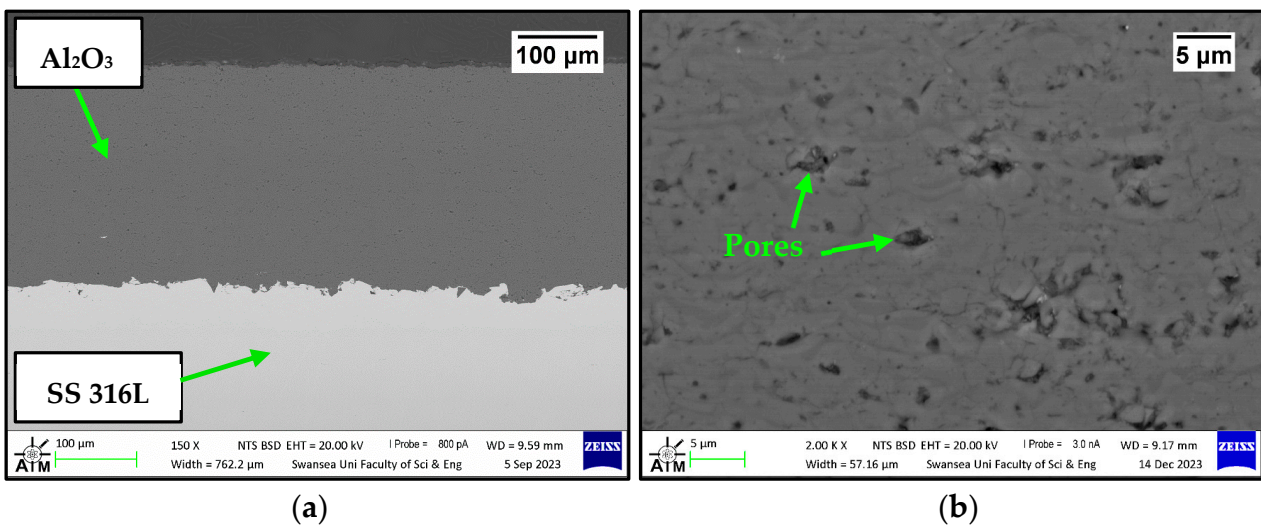


Figure 2. (a) Cross section of the as-received specimen; (b) details of pores in the Al<sub>2</sub>O<sub>3</sub> coating.

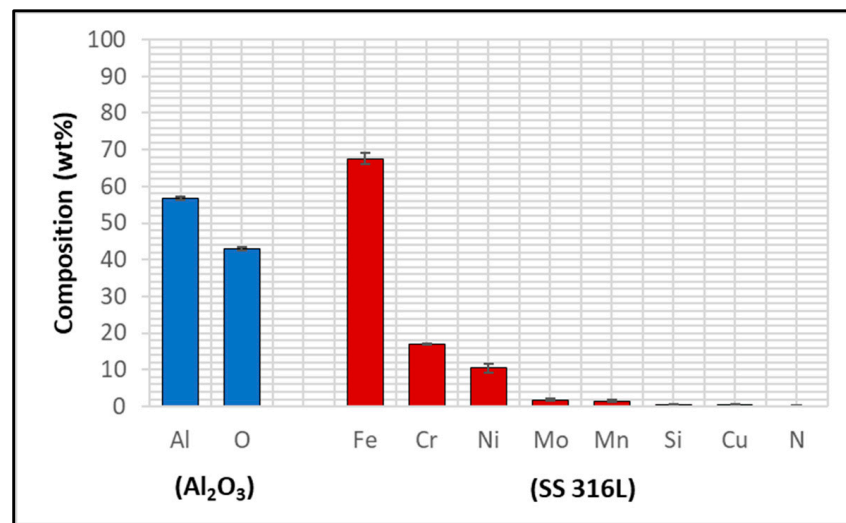


Figure 3. EDS analysis of the as-received specimens.

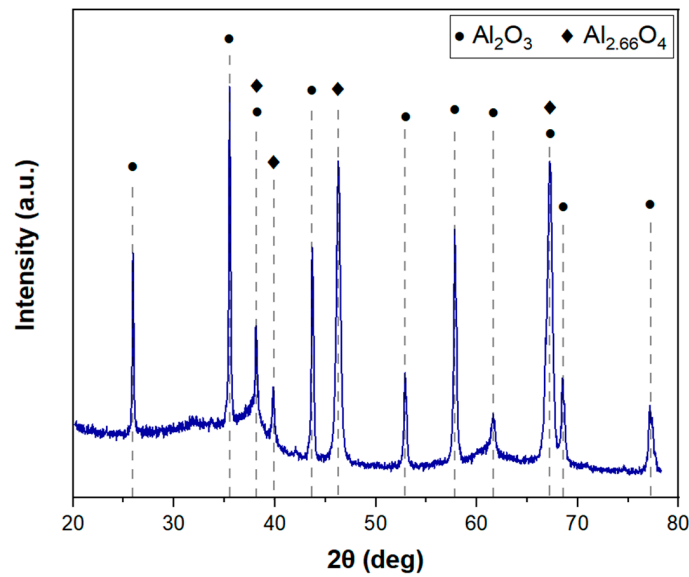


Figure 4. X-ray diffraction patterns for as-received Al<sub>2</sub>O<sub>3</sub> coatings.

### 3.2. Static Testing

#### 3.2.1. Immersion Tests in Zn-Al

SS 316L was characterised after 5 weeks of immersion in Zn-Al, and the cross-section of the specimen is shown in Figure 5a. The SEM image was captured on the regions of the specimen where exposure to the molten Zn alloy occurred, as the products of reactions with the Zn alloy bath were expected to be found at the interface. Figure 5a showed that SS 316L reacted with Zn-Al, and reaction products were identified at the interface, as indicated in the SEM image. The corrosion of SS 316L occurring in baths containing Zn and Al was reported in other studies [20–24]. A diffusion layer developed beneath the steel surface, and its thickness was measured to be around 30 μm, determined from an average of ten measurements taken on the analysed area. However, the thickness of the diffusion layer was nonuniform, and it was observed that the layer grew with an undulating pattern. The waviness of this pattern may be caused by the dissolution of Cr and Ni from SS 316L into the melt as the material is submerged in the Zn bath. It was theorised that the diffusion process stopped later than in others, as it took more time for an intermetallic cross particle to deposit, leading to the development of a thicker diffusion layer [25].

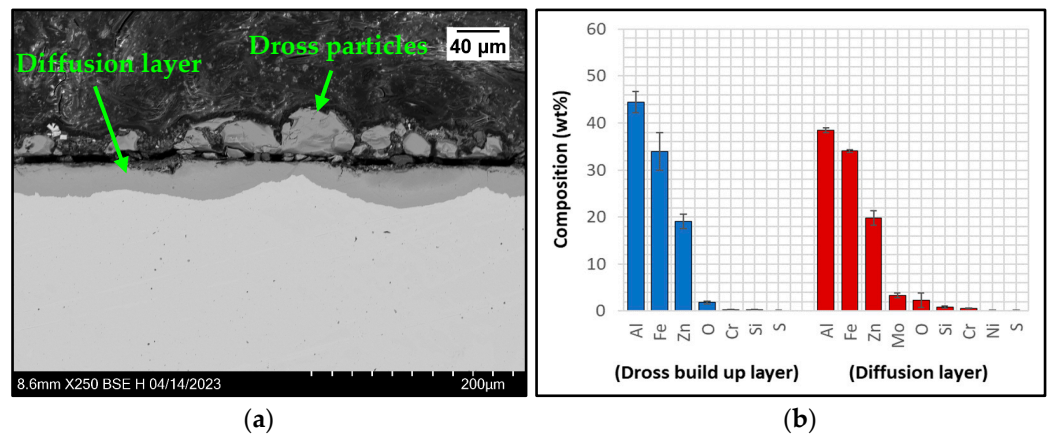


Figure 5. (a) Cross-section of SS 316L after 5 weeks of immersion in Zn-Al; (b) EDS phase elemental analysis of the reaction products observed in SS 316L after immersion in Zn-Al.

EDS phase elemental analysis was performed at different locations in this layer, and the average composition is given in Figure 5b. EDS revealed that the subsurface reaction layer mainly contained Al ( $38.4 \pm 0.5$  wt.%), Fe ( $34 \pm 0.3$  wt.%), Zn ( $19.9 \pm 1.5$  wt.%) and Mo ( $3.4 \pm 0.5$  wt.%). The formation of this layer was the result of Al diffusion from the molten metal bath into the SS 316L specimen due to the high affinity of Al for Fe [9]. It was reported that when the Al content in the bath was below 0.15 wt.%, the dominant chemical process was the Zn-Fe reaction. If the Al content was above 0.15 wt.%, the Al-Fe reaction became the dominant process, leading to the formation of a diffusion layer at the interface of SS 316L and the Zn alloy [23]. In addition to this, Figure 5a shows the presence of reaction products distributed over the surface of SS 316L. This layer was characterised by a build-up of intermetallic dross particles and was found to predominantly contain Al ( $44.4 \pm 2.3$  wt.%), Fe ( $33.9 \pm 4$  wt.%) and Zn ( $19.1 \pm 1.5$  wt.%). The thickness of the particles was measured to be approximately 30  $\mu\text{m}$ . The formation of the intermetallic particles was attributed to the dissolution of the steel by Zn. Zn reacted with the Fe from the specimen, forming a layer of intermetallic dross particles. Figure 5b suggests that the intermetallic dross particles were chemically the same as the subsurface reaction layer, except for the absence of Mo. Diffusion coefficients of Mo into liquid Zn were calculated in other studies [25], which concluded that Mo took more time to diffuse compared to the other elements present in the steel.

SEM images of the  $\text{Al}_2\text{O}_3$  coatings after 1 week and 3 weeks of testing in Zn-Al are shown in Figure 6a,b and Figure 6c,d, respectively. All the tested specimens analysed in this study were characterised by cracks that developed in the ceramic coating. Horizontal cracks started to form during the early stages of testing, as they were observed in the images captured after 1 week of exposure to molten Zn-Al. Furthermore, fragments of the coatings detached from the specimen, resulting in localised spallation, as shown in Figure 6b. It is possible to observe that the coating spalled in the proximity of a horizontal crack, as indicated in the figure. The cracks observed in the  $\text{Al}_2\text{O}_3$  coatings after static immersion testing were not present in the untested specimen, as shown in Figure 2. Therefore, they developed after exposure to molten metal at high temperatures. Unlike the uncoated SS 316L specimen, no products of reactions between SS 316L and liquid Zn-Al were observed, suggesting that  $\text{Al}_2\text{O}_3$  is capable of protecting the steel from the attack of liquid Zn-Al after 1 week of testing. Moreover, the  $\text{Al}_2\text{O}_3$  coating was found to remain inert to liquid Zn-Al, as no reaction products accumulated at the interface between the ceramic and the molten metal. However, the presence of cracks in the  $\text{Al}_2\text{O}_3$  coating could be detrimental to the performance of the materials in liquid Zn alloy if Zn infiltration through these cracks and subsequent reaction with SS 316L occurred.

After 3 weeks of testing in Zn-Al, severe coating degradation occurred. Both horizontal cracks and vertical cracks were observed in the ceramic coating. The large horizontal crack observed in Figure 6c shows that most of the coating detached from the steel substrate, leaving the surface of the steel protected only by a thin ( $\sim 20$   $\mu\text{m}$ ) layer of  $\text{Al}_2\text{O}_3$ , which again prevented the formation of corrosion products on the steel. Figure 6d shows that the breakdown of the  $\text{Al}_2\text{O}_3$  coating occurred, as fragments of the coatings were observed in the SEM image. The bright phase detected between the coating fragments and the steel was residual Zn-Al, which solidified upon removal of the specimen from the molten metal bath; its presence suggested that liquid Zn-Al reached the surface of the steel specimen, causing it to be exposed to molten metal. As a result, a reaction layer developed (Figure 7a) in a similar fashion to that seen on the uncoated SS 316L specimen previously discussed (Figure 5a). EDS phase elemental analysis (Figure 7b) revealed that the diffusion layer mainly contained Al ( $41 \pm 0.6$  wt.%), Fe ( $29.7 \pm 1.1$  wt.%) and Zn ( $19.9 \pm 1$  wt.%), and its composition was similar to that observed previously in the uncoated SS 316L specimen (Figure 5b).

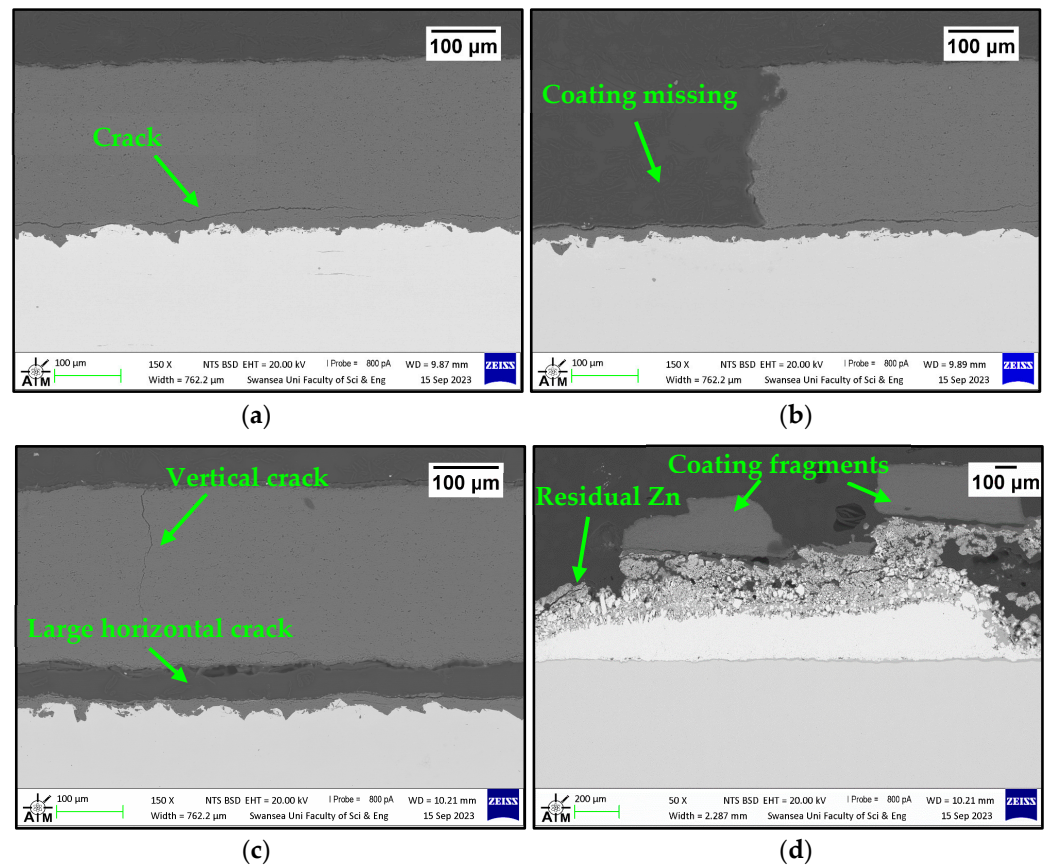


Figure 6. Cross-sections of Al<sub>2</sub>O<sub>3</sub> coated SS 316L after 1 week (a,b) and 3 weeks (c,d) of static immersion testing in Zn-Al.

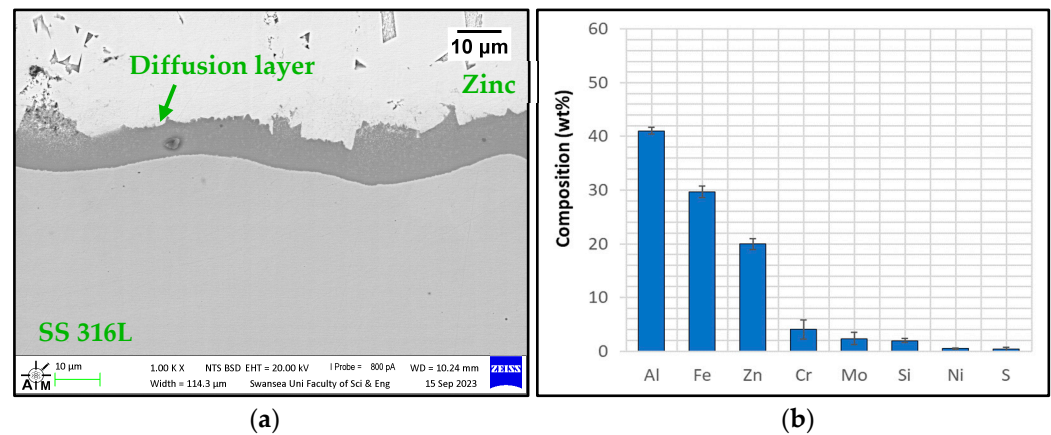
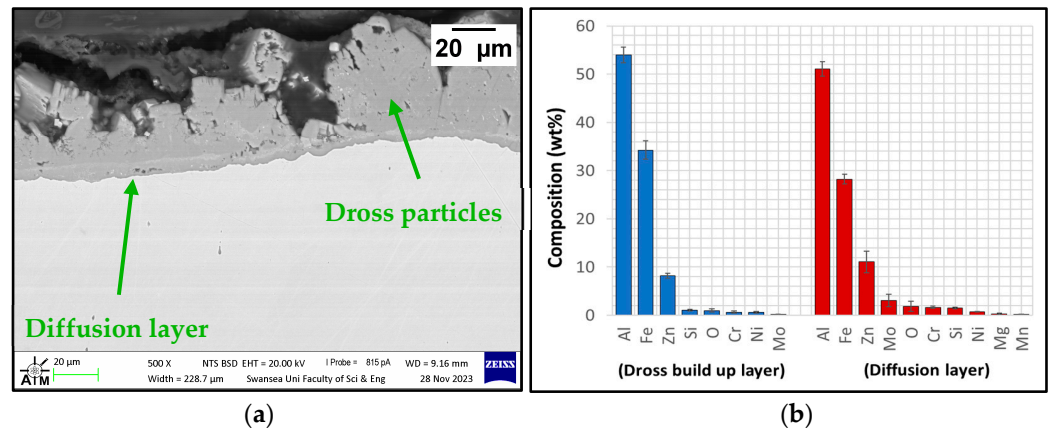


Figure 7. (a) Details of the diffusion layer observed after the breakdown of the Al<sub>2</sub>O<sub>3</sub> coating and subsequent contact with Zn-Al; (b) EDS phase elemental analysis of the diffusion layer.

### 3.2.2. Immersion Tests in Zn-Al-Mg

Figure 8a shows a cross-section of the uncoated SS 316L after immersion in Zn-Al-Mg for 5 weeks. SS 316L reacted with the Zn-Al-Mg, and corrosion products were identified at the interface, as was observed in the specimen tested in Zn-Al. A diffusion layer developed beneath the steel surface, again following an undulating pattern. The results of the EDS phase elemental analysis of this layer are shown in Figure 8b. It was found that the composition of this layer was similar to that of the specimen immersed in Zn-Al, as it mainly contained Al (51.1 ± 1.5 wt.%), Fe (28.24 ± 1 wt.%) and Zn (11.1 ± 2.3 wt.%). However, it was observed that the diffusion layer in the Zn-Al-Mg bath was significantly

thinner than that of the sample immersed in the Zn-Al bath. EDS analysis showed that the diffusion layer in the sample immersed in the Zn-Al contained a higher amount of Zn (20%) compared to the diffusion layer measured in the sample immersed in Zn-Al-Mg (~8%). The Al levels were measured to be ~10% higher in the Zn-Al-Mg bath than in the Zn-Al bath.



**Figure 8.** (a) Cross-section of SS 316L after 5 weeks of immersion in Zn-Al-Mg; (b) EDS phase elemental analysis of the reaction products observed in SS 316L after immersion in Zn-Al-Mg.

A number of studies observed that there was a relationship between the Al content in the liquid Zn bath and the formation of FeZn compounds [23,26,27]. The Al was found to delay the FeZn reaction by segregating to the surface of the steel and forming an ‘inhibition layer’. In addition to this, the time for the FeZn phases to develop increased with increasing levels of Al in the bath. Since the Zn-Al-Mg bath used in this study contained ten times more Al than the Zn-Al bath, it was concluded that the higher Al levels reduced the diffusion of Zn into the SS 316L specimen, leading to the formation of a thinner reaction layer. Therefore, the Zn-Al-Mg bath composition provided greater inhibition of the reaction between the SS 316L and the molten Zn in the bath.

SEM images of the Al<sub>2</sub>O<sub>3</sub> coatings after 4 weeks of immersion in Zn-Al-Mg are shown in Figure 9. Some similarities were observed with the specimens immersed in Zn-Al, such as spallation and breakdown of the coatings (Figure 9a), as well as the presence of cracks (Figure 9b). It is evident from Figure 9b,c that the liquid Zn alloy penetrated through cracks that formed in the coating. Moreover, contact occurred between the steel and the molten metal, as observed in the specimens immersed in Zn-Al. This contact was facilitated by the spallation of the Al<sub>2</sub>O<sub>3</sub> coating, which exposed SS 316L to the attack of the liquid Zn-Al-Mg. Consequently, corrosion products are formed on the surface of SS 316L. However, further degradation was detected on the coatings immersed in the Zn-Al-Mg bath. Figure 9 shows that certain regions of the coatings deteriorated in molten metal, whereas other areas remained unaffected (Figure 9b). These areas were identified in the proximity of the surfaces where contact with Zn occurred, as well as near cracks where liquid Zn alloy permeated, suggesting that the Al<sub>2</sub>O<sub>3</sub> coatings interacted with the molten Zn-Al-Mg. The details of these interactions are shown in Figure 9d, and the SEM image showed three phases: a light phase, which was the Zn that penetrated through pores and cracks present in the coating; a dark grey phase, which was the Al<sub>2</sub>O<sub>3</sub> in the coating; a light grey phase, which was a new phase as it was absent in the as-received Al<sub>2</sub>O<sub>3</sub> coating (Figure 2). In addition to this, the new phase was absent in all the coatings tested in the Zn-Al bath. Therefore, its formation is likely to be related to the presence of Mg in the Zn-Al-Mg bath.

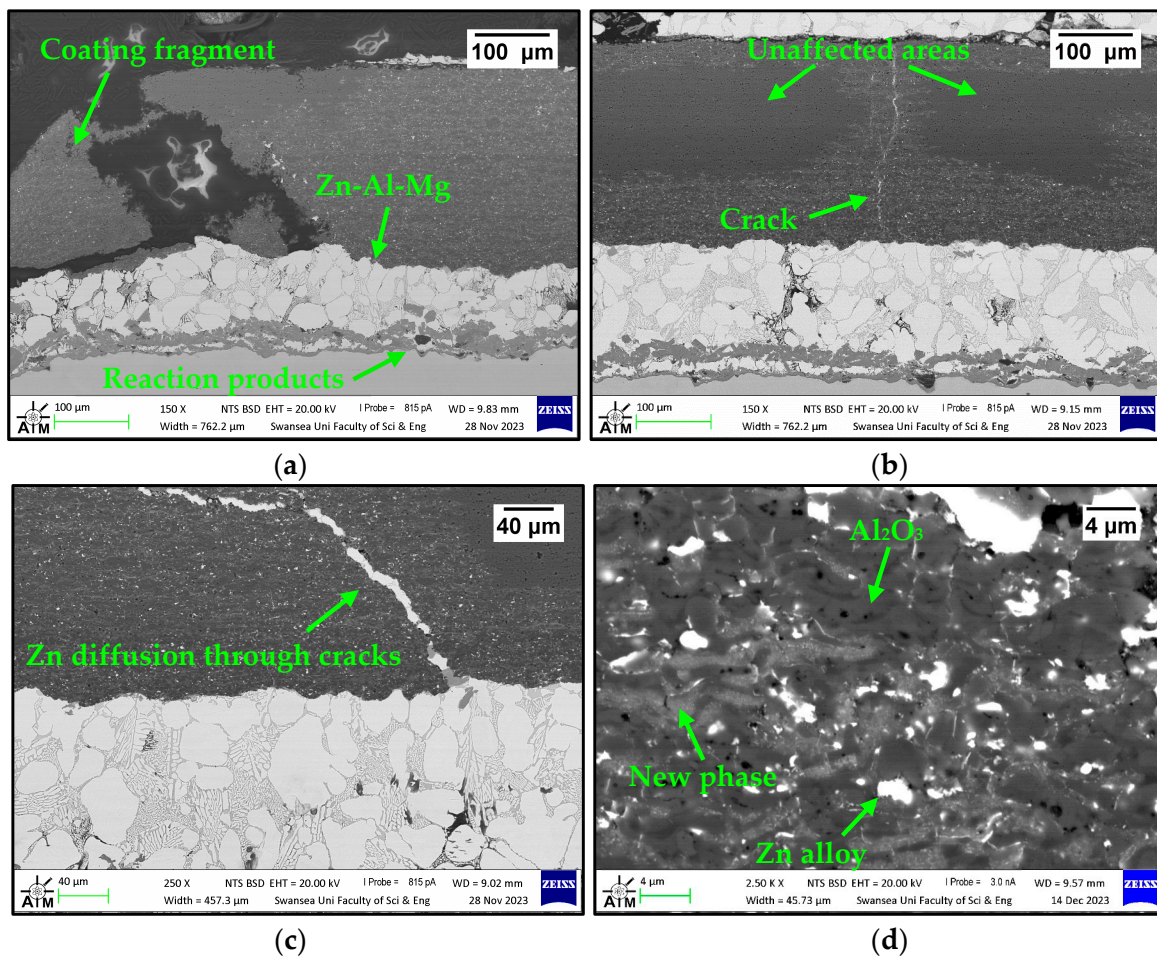


**Figure 9.** Cross-sections of the  $\text{Al}_2\text{O}_3$  coatings after 4 weeks of immersion in Zn-Al-Mg: (a) spallation of the coating; (b) details of cracks and areas of the coating affected by degradation in molten metal; (c) Zn diffusion through cracks; (d) details of the three phases.

To confirm this, EDS mapping was performed in the regions of the coatings where the new phase was detected, and the results are shown in Figure 10. It was observed that some areas of the coating were rich in Mg; these areas corresponded to the new phase. Moreover, the analysis showed that the new phase was low in Al, suggesting that a reaction occurred with the molten metal bath. It is postulated that  $\text{Al}_2\text{O}_3$  was reduced by the Mg present in the bath, forming MgO in the coating. It is well known that  $\text{Al}_2\text{O}_3$  can be reduced by Mg metal following the reaction  $3\text{Mg} + \text{Al}_2\text{O}_3 = 2\text{Al} + 3\text{MgO}$ . According to the Ellingham diagram, the free energy of the formation of Mg is more negative than Al at  $465^\circ\text{C}$ , and the line for the  $2\text{Mg} + \text{O}_2 = 2\text{MgO}$  reaction lies below the  $4/3\text{Al} + \text{O}_2 = 2/3\text{Al}_2\text{O}_3$  reaction [28–30]. This observation suggested that MgO formed in the coatings after submergence in Zn-Al-Mg and can explain the results obtained from the EDS analysis. The reduction of  $\text{Al}_2\text{O}_3$  by molten Mg does not normally occur at low temperatures due to slow kinetics. However, the cracks and pores observed in this study may have provided ‘diffusion channels’ for Mg metal and led to an increase in the surface area of  $\text{Al}_2\text{O}_3$ . As a result, the higher surface area is considered to have improved the kinetics of the reduction reaction.

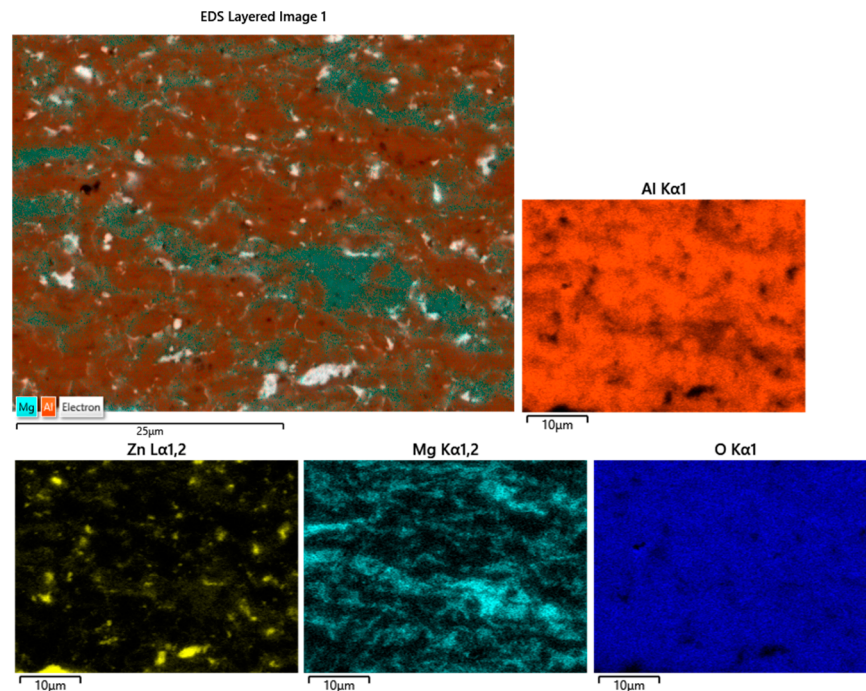


**Figure 10.** EDS maps of  $\text{Al}_2\text{O}_3$  coating after immersion in Zn-Al-Mg.

### 3.2.3. Analysis of Coating Failure

The results of static immersion testing revealed that the  $\text{Al}_2\text{O}_3$  coatings were damaged in the molten metal bath, even when no reaction between the ceramic and the liquid Zn alloy was observed, as shown in the specimens immersed in Zn-Al. Material characterisation of the coatings after exposure to molten metal at high temperatures has identified the presence of cracks that developed in the ceramic coating. The formation of cracks in ceramic and cermet coatings after exposure to high temperatures was reported in other studies in the literature [12,15,31,32]. In addition to this, cracking was linked to stress generated between materials with dissimilar CTE values [18,33]. Therefore, the cause for the development of cracks was attributed to the thermal expansion mismatch between the coating and substrate materials, which resulted in the formation of stresses responsible for inducing the cracking. In this study, dilatometry was performed to measure the CTE of  $\text{Al}_2\text{O}_3$  and SS 316L at a temperature analogous to that of each Zn bath used for the static tests (Figure 11). The CTEs recorded at  $\sim 465^\circ\text{C}$  for  $\text{Al}_2\text{O}_3$  and SS 316L were  $8.2 \times 10^{-6}$  and  $21.2 \times 10^{-6} \text{K}^{-1}$ , respectively, suggesting that the steel substrate expanded more than the  $\text{Al}_2\text{O}_3$  coating due to its higher CTE. The difference in CTE of  $13 \times 10^{-6} \text{K}^{-1}$  between the two materials caused a thermal expansion mismatch and generated tensile stresses, which probably made the ceramic coating prone to vertical cracking. In addition to this, the larger expansion of the steel substrate relative to the ceramic coating resulted in horizontal cracks near the interface between  $\text{Al}_2\text{O}_3$  and SS 316L, triggering the delamination effects previously discussed.

SEM images of the coatings showed that a breakdown of the coating occurred, and a possible failure mechanism was identified. As the specimens were immersed in the molten metal bath, contact with liquid Zn alloy occurred. Due to the high temperature and the large difference between the CTE of the substrate and coating material, cracks started to develop in the  $\text{Al}_2\text{O}_3$  coating. These cracks acted as ‘channels’ for liquid Zn alloy to diffuse in the ceramic coating and to reach the underlying steel substrate. When the steel became exposed to the attack of liquid Zn alloy, corrosion products started to form below the coating. The accumulation of these reaction products led to the generation of stresses, and the coating was forced to detach, as illustrated in Figure 6d. This potential failure mechanism was observed in other studies investigating the performance of ceramic coatings in liquid Zn [15]. It was previously shown that the  $\text{Al}_2\text{O}_3$  coatings remained

inert in liquid Zn-Al and shielded SS 316L from the attack of molten metal until coating breakdown occurred. Therefore, they have the potential to increase the service life of the bearings beyond the current five-week campaign for the production of Zn-Al coatings. However, optimisation of the ceramic coatings/substrate system is required to prevent cracking and breakdown, such as producing multilayer or composition gradient coatings to minimise the mismatch with the substrate material [9,12,34].

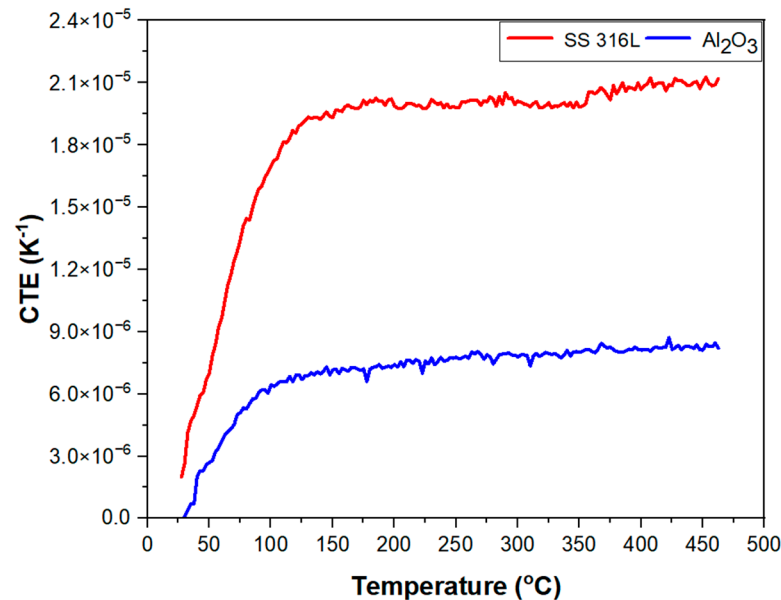


Figure 11. CTE of SS 316L and Al<sub>2</sub>O<sub>3</sub> as a function of temperature in the range of 35–465 °C.

#### 4. Conclusions

In this study, Al<sub>2</sub>O<sub>3</sub> coatings were investigated with the aim of developing galvanising pot roll bearings with extended durability in liquid Zn alloys. Static testing was conducted to compare the performance of the Al<sub>2</sub>O<sub>3</sub> coatings against that of uncoated SS 316L specimens. The corrosion behaviour of the coatings was studied after exposure to Zn-Al and Zn-Al-Mg galvanising baths. The following was concluded:

- Uncoated SS 316L specimens reacted during exposure to Zn-Al and Zn-Al-Mg as diffusion layers were detected at the steel-Zn interface, confirming that the use of uncoated SS 316L hardware in the hot-dip galvanising bath is not recommended. In the Zn-Al-Mg bath, the corrosion of SS 316L was less severe than in the Zn-Al bath due to the higher Al content of approximately 10%.
- The Al<sub>2</sub>O<sub>3</sub> coatings were damaged following exposure to molten metal at high temperatures. The difference between the CTEs of Al<sub>2</sub>O<sub>3</sub> and SS 316L was approximately  $13 \times 10^{-6} \text{ K}^{-1}$  and led to stress-induced cracking, which could be detrimental to the service life of the bearings, as they provided paths for the liquid Zn alloy to permeate and react with the SS 316L. As a result, spallation and breakdown of the Al<sub>2</sub>O<sub>3</sub> coatings occurred.
- Unlike SS 316L, the Al<sub>2</sub>O<sub>3</sub> coatings showed excellent corrosion resistance after immersion in Zn-Al; however, examination of the coatings immersed in Zn-Al-Mg revealed possible interactions with the molten metal bath due to the reduction of Al<sub>2</sub>O<sub>3</sub> by molten Mg. Therefore, the use of bearings coated with Al<sub>2</sub>O<sub>3</sub> should be limited to hot-dip galvanising baths containing Zn-Al composition in order to avoid coating degradation and the risk of incurring frequent line stops.

The resistance of the Al<sub>2</sub>O<sub>3</sub> coatings to damage by the molten Zn alloy baths holds promise that ceramic coatings can be used in the development of new bearing coatings for galvanising, although the tendency of the coating to fail due to the mismatched CTEs

of the coating and the underlying substrate requires further investigation of an optimal coating/substrate coupling to be undertaken.

**Author Contributions:** Conceptualisation, G.P.A., D.P., J.S., J.E. and C.M.; methodology, G.P.A. and D.P.; software, G.P.A.; validation, G.P.A.; formal analysis, G.P.A.; investigation, G.P.A.; resources, G.P.A., D.P., J.S., J.E. and C.M.; data curation, G.P.A.; writing—original draft preparation, G.P.A.; writing—review and editing, G.P.A., D.P., J.S., J.E. and C.M.; visualisation, G.P.A.; supervision, D.P., J.S. and C.M.; project administration, D.P., J.S., J.E. and C.M.; funding acquisition, D.P., J.S., J.E. and C.M. All authors have read and agreed to the published version of the manuscript.

**Funding:** This project was supported by the Engineering and Physical Sciences Research Council (Grant Ref: EP/V519601/1) with Tata Steel.

**Institutional Review Board Statement:** Not applicable.

**Informed Consent Statement:** Not applicable.

**Data Availability Statement:** Data are contained within the article.

**Acknowledgments:** The authors would like to thank Engineered Performance Coatings (EPC), Cardiff, and The Steel and Metals Institute (SaMI) and The Advanced Imaging Facility (AIM) at Swansea University. Moreover, we thank Shahin Mehraban, Swansea University, for the measurement of the CTE, and Clive Challinor, Tata Steel, for advice on the utilisation of bearings in galvanised steel production.

**Conflicts of Interest:** The authors declare no conflict of interest. The funders had no role in the design of the study; in the collection, analyses, or interpretation of data; in the writing of the manuscript; or in the decision to publish the results.

## References

1. Gossuin, T.; Moreas, G. Cleanliness Measurement by Innovative Libs Method. In Proceedings of the 12th International Conference on Zinc and Zinc Alloy Coated Steel Sheet (Galvatech), Virtual Conference, Online, 21–23 June 2021.
2. Beentjes, P.; Bottema, J.; Salgin, B.; Vrenken, J. An Innovative GI with Improved Gallling and Surface Properties for Exposed Automotive Applications. In Proceedings of the 12th International Conference on Zinc and Zinc Alloy Coated Steel Sheet, Virtual Conference, Online, 21–23 June 2021.
3. Tang, N.Y.; Daniel, L.; Zhang, K. Performance of Submerged Hardware in Continuous Galvanizing. *Corros. Sci. Technol.* **2010**, *9*, 116–121.
4. Zhang, K.; Tang, N.Y.; Goodwin, F. Research and development of pot bearings in continuous galvanizing. In Proceedings of the 6th International Conference on Zinc and Zinc Alloy Coated Steel Sheet, Chicago, IL, USA, 4–7 April 2004.
5. Zhang, K. Effects of test conditions on the tribological behaviour of a journal bearing in molten zinc. *Wear* **2005**, *259*, 1248–1253. [[CrossRef](#)]
6. Marder, A.; Goodwin, F. *The Metallurgy of Zinc Coated Steels*; Elsevier: Cambridge, MA, USA, 2023.
7. Escott, L.J.; Penney, D.J.; Das, A.; Thomas, D. Effects of Heat Treatments on the Morphology and Mechanical Properties of a CoCrW Alloy for Hot Dip Galvanising Applications. In Proceedings of the 12th International Conference on Zinc and Zinc Alloy Coated Steel Sheet, Virtual Conference, Online, 21–23 June 2021.
8. Faulkner, R.; Penney, D.; Bright, M. Offline Simulation of Galvanising Bath Journal Bearings as a Cost Effective Solution to Improve Line Performance and Mitigate Risk. In Proceedings of the 12th International Conference on Zinc & Zinc Alloy Coated Steel Sheet, Virtual Conference, Online, 21–23 June 2021.
9. Matthews, S.J.; James, B. Review of Thermal Spray Coating Applications in the Steel Industry: Part 2—Zinc Pot Hardware in the Continuous Galvanizing Line. *J. Therm. Spray Technol.* **2010**, *19*, 1277–1286. [[CrossRef](#)]
10. Shi, Y.; Tong, J.; Zheng, Q.; Rao, S.; Jin, H.; Rao, S. Analysis About the Failure Mechanism of the Sleeves in Sink Roll System. *J. Fail. Anal. Prev.* **2018**, *18*, 183–188. [[CrossRef](#)]
11. Nag, A.; Bhadu, M.K.; Bijalwan, P.K.; Pathak, A.S. Investigation of selected HVOF and plasma sprayed coatings for sustained performance in molten zinc. *Corros. Sci.* **2021**, *180*, 109177. [[CrossRef](#)]
12. Dong, Y.; Yan, D.; He, J.; Zhang, J.; Li, X. Degradation behaviour of ZrO<sub>2</sub>-Ni/Al gradient coatings in molten Zn. *Surf. Coat. Technol.* **2006**, *201*, 2455–2459. [[CrossRef](#)]
13. Jarosinski, W.; Quets, J.; Wang, D.; Belov, V.; Klyrman, A.S. Thermal Spray Coated Rolls for Molten Metal Baths. U.S. Patent 8,507,105 B2, 13 August 2013.
14. Liu, X.; Zhao, X.; Yang, F. Room-Temperature and High-Temperature Wear Behaviors of As-Sprayed and Annealed Cr<sub>3</sub>C<sub>2</sub>-25NiCr Coatings Prepared by High Velocity Air-Fuel Spraying. *Coatings* **2020**, *10*, 1090. [[CrossRef](#)]

15. Wang, Q.; Zhang, J.W.; Zhang, L.; Liu, H.J.; Zeng, C.L. Stability investigation of electrodeposited zirconium diboride ceramic coatings in molten zinc. *Mater. Corros.* **2019**, *70*, 492–502. [[CrossRef](#)]
16. Chakraborty, A.; Ghassemi-Armaki, H. Evaluation of Initiation and Propagation of LME Cracks on the Galvanised 3G-AHSS Using Interrupted Resistance Spot-Welding Method. In Proceedings of the 12th International Conference on Zinc and Zinc Alloy Coated Steel Sheet, Virtual Conference, Online, 21–23 June 2021.
17. Gražulis, S.; Chateigner, D.; Downs, R.; Yokochi, A.; Quirós, M.; Lutterotti, L.; Manakova, E.; Butkus, J.; Moeck, P.; Le Bail, A. Crystallography Open Database—An Open-Access Collection of Crystal Structures. *J. Appl. Crystallogr.* **2009**, *42*, 726–729. [[CrossRef](#)]
18. Huang, W.; Qiu, H.; Zhang, Y.; Zhang, F.; Gao, L.; Omran, M.; Chen, G. Microstructure and phase transformation behavior of  $\text{Al}_2\text{O}_3\text{-ZrO}_2$  under microwave sintering. *Ceram. Int.* **2023**, *49*, 4855–4862. [[CrossRef](#)]
19. Kaunisto, K.; Lagerbom, J.; Honkanen, M.; Varis, T.; Lambai, A.; Mohanty, G.; Levänen, E.; Kivikytö-Reponen, P.; Frankberg, E. Evolution of alumina phase structure in thermal plasma processing. *Ceram. Int.* **2023**, *49*, 21346–21354. [[CrossRef](#)]
20. Zhang, K.; Tang, N.-Y.; Goodwin, F.E.; Sexton, S. Reaction of 316L stainless steel with a galvanizing bath. *J. Mater. Sci.* **2007**, *42*, 9736–9745. [[CrossRef](#)]
21. Khaliq, A.; Alghamdi, A.S.; Ramadan, M.; Subhani, T.; Rajhi, W.; Haider, W.; Hasan, M.M. Intermetallic Compounds Formation during 316L Stainless Steel Reaction with Al-Zn-Si Coating Alloy. *Crystals* **2022**, *12*, 735. [[CrossRef](#)]
22. Yu, Z.; Chen, M.; Wang, J.; Li, F.; Zhu, S.; Wang, F. Enamel coating for protection of the 316 stainless steel against tribo-corrosion in molten zinc alloy at 460 °C. *J. Mater. Sci. Technol.* **2021**, *65*, 126–136. [[CrossRef](#)]
23. Liu, X.; Barbero, E.; Xu, J.; Burriss, M.; Chang, K.-M.; Sikka, V. Liquid metal corrosion of 316L,  $\text{Fe}_3\text{Al}$ , and FeCrSi in molten Zn-Al baths. *Metall. Mater. Trans. A* **2005**, *36*, 2049–2058. [[CrossRef](#)]
24. Yu, Z.; Chen, M.; Li, F.; Zhu, S.; Wang, F. Synergistic effect of corrosion and wear of the 316 stainless steel in molten zinc alloy at 460 °C. *Corros. Sci.* **2020**, *165*, 108411. [[CrossRef](#)]
25. Kuperus, M. The Delamination Process of the Dross Build-Up Structure on Submerged Hardware in Zn-Al and Zn-Mg-Al Baths: An Empirical Study. Master's Thesis, Delft University of Technology, Delft, The Netherlands, 2018.
26. Marder, A.R. The metallurgy of zinc-coated steel. *Prog. Mater. Sci.* **2000**, *45*, 191–271. [[CrossRef](#)]
27. Bright, M.A. Dissolution and Diffusion Characteristics of 316L Stainless Steel in Molten Zinc Containing Variable Concentrations of Aluminum. Master's Thesis, West Virginia University, Morgantown, WV, USA, 2007.
28. Liu, J.; Suryanarayana, C.; Ghosh, D.; Subhash, G.; An, L. Synthesis of Mg- $\text{Al}_2\text{O}_3$  nanocomposites by mechanical alloying. *J. Alloys Compd.* **2013**, *563*, 165–170. [[CrossRef](#)]
29. Zhang, J.; Liu, Y.; Babamiri, B.B.; Zhou, Y.; Dargusch, M.; Hazeli, K.; Zhang, M.-X. Enhancing specific energy absorption of additively manufactured titanium lattice structures through simultaneous manipulation of architecture and constituent material. *Addit. Manuf.* **2022**, *55*, 102887. [[CrossRef](#)]
30. University of Cambridge. Dissemination of IT for the Promotion of Materials Science (DoITPoMS). Available online: [https://www.doitpoms.ac.uk/tlplib/ellingham\\_diagrams/ellingham.php](https://www.doitpoms.ac.uk/tlplib/ellingham_diagrams/ellingham.php) (accessed on 19 March 2024).
31. Noda, N.-A.; Yamada, M.; Sano, Y.; Sugiyama, S.; Kobayashi, S. Thermal stress for all-ceramics rolls used in molten metal to produce stable high quality galvanized steel sheet. *Eng. Fail. Anal.* **2008**, *15*, 261–274. [[CrossRef](#)]
32. Mizuno, H.; Kitamura, J. MoB/CoCr Cermet Coatings by HVOF Spraying against Erosion by Molten Al-Zn Alloy. *J. Therm. Spray Technol.* **2007**, *16*, 404–413. [[CrossRef](#)]
33. Huang, W.; Zhang, Y.; Lu, J.; Gao, L.; Zhang, F.; Chen, J.; Omran, M.; Chen, G. Effect of sintering time on the microstructure and stability of  $\text{Al}_2\text{O}_3\text{-ZrO}_2$  composite powders under microwave-assisted sintering. *Ceram. Int.* **2023**, *49*, 8993–8999. [[CrossRef](#)]
34. Mizuno, H.; Kitamura, J. Thermal Spray Coating and Thermal Spray Powder. U.S. Patent 7,862,911 B2, 4 January 2011.

**Disclaimer/Publisher's Note:** The statements, opinions and data contained in all publications are solely those of the individual author(s) and contributor(s) and not of MDPI and/or the editor(s). MDPI and/or the editor(s) disclaim responsibility for any injury to people or property resulting from any ideas, methods, instructions or products referred to in the content.